RSC Advances

PAPER

View Article Online
View Journal | View Issue

Check for updates

Cite this: *RSC Adv.*, 2019, **9**, 13077

Highly efficient & stable Bi & Sb anodes using lithium borohydride as solid electrolyte in Li-ion batteries†

Pooja Kumari,[ab] Khushbu Sharma,[ab] Pratibha Pal,[a] Manoj Kumar,[b] Takayuki Ichikawa *[a] and Ankur Jain *[c]

Received 27th February 2019
Accepted 15th April 2019

DOI: 10.1039/c9ra01479a

rsc.li/rsc-advances

Herein, we employed Bi and Sb as the negative electrode in all solid-state lithium-ion batteries (LIBs) using $LiBH_4$ as the solid-state electrolyte. The composite anode materials with acetylene black (AB) and $LiBH_4$, prepared by high energy ball-milling, have shown extremely high stability with a high coulombic efficiency of 90–99% over a number of cycles. The gravimetric capacity decayed by only 18 and 5% as compared to the initial volumetric capacity of 4681.7 and 4393.4 mA h cm^{-3} for Bi and Sb anodes respectively.

Open Access Article. Published on 29 April 2019. Downloaded on 2/1/2026 9:02:21 AM.
This article is licensed under a Creative Commons Attribution-NonCommercial 3.0 Unported Licence.

At present, all solid state batteries are evolving rapidly because of the volatile and flammable nature of liquid electrolytes, which is one of the critical factors resulting in the safety issues of LIBs. The all solid-state battery replaces the flammable organic liquid electrolytes with a suitable solid-state electrolyte and allows the operation temperature for batteries to be increased, which can effectively improve the reaction kinetics. Although a huge number of solid state electrolytes have been explored, $LiBH_4$ has been investigated very intensively due to its remarkably high Li^+ conductivity in the order of 10^{-3} S cm^{-1} for its high-temperature phase around 120 °C.[1,2] Despite its high ionic conductivity, $LiBH_4$ has been employed only for hydride material as a solid state electrolyte so far[3,4] as it was believed that the reaction kinetics could be enhanced due to H–H exchange between $LiBH_4$ and the hydride material.[5] In order to extend the use of $LiBH_4$ with other electrode materials and establish it as a universal solid electrolyte, it is necessary to investigate its compatibility with other materials. Graphite has been widely accepted as commercial anode material, however it has several limitations, *e.g.*, its low theoretical capacity (372 mA h g^{-1}), and safety issues due to its low reaction potential with Li. Therefore, it is vital to develop other suitable anode candidates to react with Li to deliver high capacities and higher potential for LIBs.[6] In order to replace the graphite, several alternative anode materials such as Si, Ge, Sn, P, metal oxides, *etc.* have attracted attention due to the alloys formation in a much higher mole ratio at safer potentials. Besides, these anodes can deliver much higher capacities, *i.e.* 2–10 times more than that of commercially adopted graphite.[7] However, at the same time, these materials are hampered by the structural instabilities caused by drastic volumetric changes of up to 150–400% upon full lithiation. As compared to the other group elements, Sb has been considered as a favourable anode material because of less volume expansion during the electrochemical process in LIBs.[8] Furthermore, Sb exhibits high energy density due to its high theoretical capacity of 660 mA h g^{-1} upon full lithiation to Li_3Sb and very high volumetric capacity (4420 mA h cm^{-3} in comparison with 843 mA h cm^{-3} for graphite), on account of its two-dimensional puckery layered structure, such a structure is thought to be favourable to promise high electrical conductivity.

Also, bismuth (Bi) deserves to be discussed in terms of its lithium storage performance because of being the element from the same group as Sb. Bi is relatively more stable in the moisture/air atmosphere at room temperature than other alloying materials and can deliver sufficiently high gravimetric capacity (386 mA h g^{-1}) with a very high volumetric capacity (3765 mA h cm^{-3}). The above key points make it a promising anode material for LIBs and several studies have been carried out to improve its properties as a negative electrode.[9–13] Both the materials (Bi & Sb) have been studied with different liquid electrolytes so far, however are not employed yet in all-solid-state batteries to the best of our knowledge. In this communication, we are presenting the first ever electrochemical performance of all-solid-state Li-ion battery using Bi and Sb as anode and $LiBH_4$ as a solid electrolyte. To obtain the fast Li^+ conduction from $LiBH_4$, all the electrochemical measurements in this manuscript were performed at 120 °C.

[a]*Graduate School of Engineering, Hiroshima University, Higashi-Hiroshima 739-8527, Japan. E-mail: tichi@hiroshima-u.ac.jp*

[b]*Department of Physics, Malaviya National Institute of Technology Jaipur, Rajasthan-302017, India*

[c]*Natural Science Centre for Basic Research and Development, Hiroshima University, Higashi-Hiroshima 739-8521, Japan. E-mail: ankur.j.ankur@gmail.com*

† Electronic supplementary information (ESI) available. See DOI: 10.1039/c9ra01479a

Open Access Article. Published on 29 April 2019. Downloaded on 2/1/2026 9:02:21 AM.
This article is licensed under a Creative Commons Attribution-NonCommercial 3.0 Unported Licence.

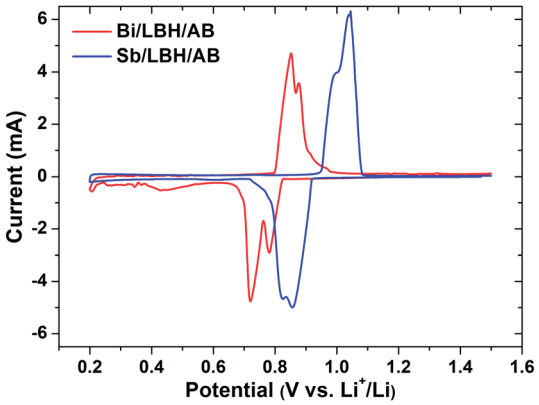

Fig. 1 Cyclic voltammograms of Bi and Sb composite electrode scanned at 0.1 mV s^{-1}.

Fig. 1 shows the CV scan profiles of the Bi and Sb electrodes at 0.1 mV s^{-1} between 0.2 V to 1.5 V (Li^+/Li) potential window. At first, during the lithiation (discharging) scan of Bi/$LiBH_4$/AB electrode, the broad peak composing of two peaks located at about 0.79 V and 0.72 V is expected to be the alloying reaction of Bi to LiBi and Li_3Bi phases respectively as per the theoretical voltage values. Turn to the charging process, anodic peaks at around 0.85 V and 0.88 V exhibit the delithiation reactions of Li_3Bi returning to metallic Bi through LiBi acting as an intermediate state. Similarly, the CV curve of Sb/$LiBH_4$/AB electrode reveals the peaks at 0.86 V and 0.82 V that correspond to the formation of Li_2Sb and Li_3Sb phases respectively, during the insertion of Li-ions and in reverse anodic scan, the peaks at 0.99 V and 1.04 V are attributed to the exertion of Li-ions from alloyed Li_3Sb phase.

Fig. 2(a) exhibits the first galvanostatic discharge–charge curves for the Bi–$LiBH_4$–AB composite electrode between the optimized potential window 0.2–1.5 V *vs.* Li^+/Li at the 0.1C rate. The other higher current rates were also tested (results are not shown here), however the performance was not found suitable. The initial discharge and charge capacity of the Bi–$LiBH_4$–AB composite is observed as 4681.7 mA h cm^{-3} (478.7 mA h g^{-1}) and 4510.5 mA h cm^{-3} (461.2 mA h g^{-1}), with an initial coulombic efficiency of 96.3%. Likewise, for Sb–$LiBH_4$–AB composite material, the first discharge–charge profile represents the initial capacity corresponding to delithiation–lithiation as 4393.4 mA h cm^{-3} (657.7 mA h g^{-1}) and 4189.7 mA h cm^{-3} (627.2 mA h g^{-1}) respectively with 95.4% coulombic efficiency [Fig. 2(b)]. To understand the mechanism behind the obtained plateaus, the *ex situ* XRD measurements were performed at selected potentials, as indicated in the galvanostatic discharging/charging profile. Since $LiBH_4$ is used as an electrolyte as well as in anode composite material with sufficient amount (30%), so the peaks corresponding to the $LiBH_4$ phase are present in XRD profile at all stages (ESI, Fig. S1 and S2†). The obtained capacity for Bi–$LiBH_4$–AB composite is slightly higher than the theoretical value, which can be attributed to the side reaction/the contribution from carbon lithiation. On the discharge curve (Li^+ incorporation into Bi), the potential gradually drops to around 0.82 V and displays a long flat plateau until point 2, where the Li-ion moves from the positive electrode (cathode) to negative electrode (anode) and reacts with Bi and makes LiBi (ESI, Fig. S1†). The next discharge plateau is observed at 0.78 V, immediately after the 1st plateau and very close to it. This plateau ends at point 3 and corresponds to the LiBi → Li_3Bi reaction (ESI, Fig. S1†). The opposite reaction occurred exactly in the opposite direction, as can be observed from the presence of two plateaus during the charging process (Li^+ extraction), which suggests a high reversibility of the reaction Li ↔ Li_3Bi. The polarization between Li insertion and extraction is <0.1 V, which is much smaller than that of the Bi electrodes with organic liquid based electrolytes. Such a low polarization can be attributed to fast diffusion of species and the high working temperature of 120 °C, which brings better kinetic properties to the Bi alloying reaction. The above results indicate that the existence of $LiBH_4$ significantly promotes the

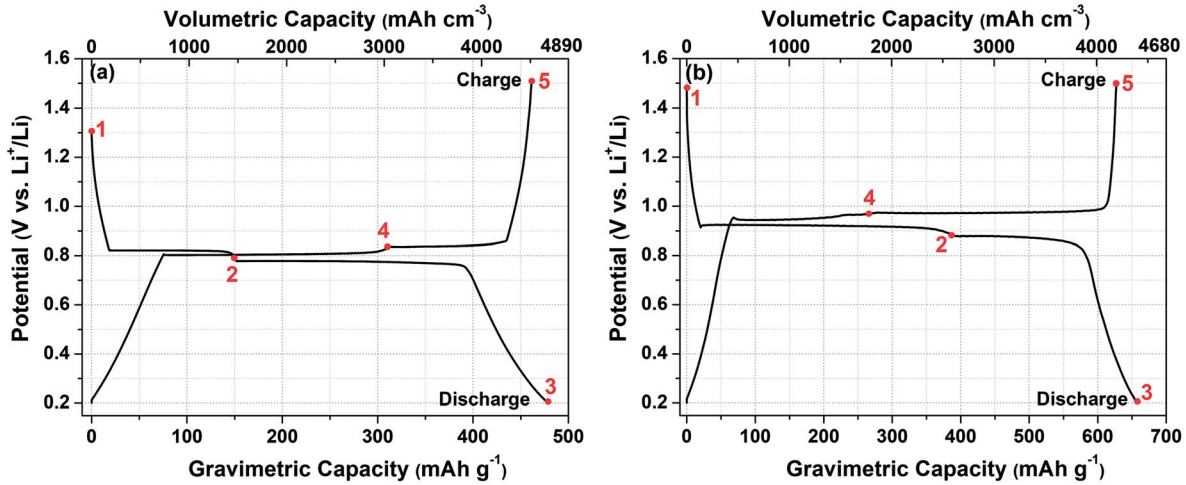

Fig. 2 The first galvanostatic discharge–charge curves for (a) Bi–$LiBH_4$–AB composite (b) Sb–$LiBH_4$–AB composite electrodes in the voltage range of 0.2–1.5 V at 0.1C.

This journal is © The Royal Society of Chemistry 2019

Open Access Article. Published on 29 April 2019. Downloaded on 2/1/2026 9:02:21 AM.
This article is licensed under a Creative Commons Attribution-NonCommercial 3.0 Unported Licence.

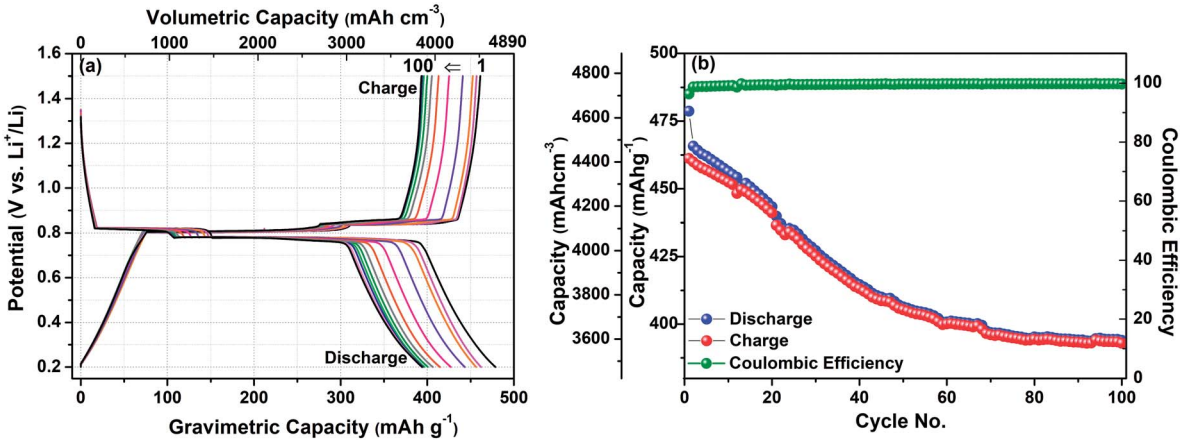

Fig. 3 (a) The cyclic galvanostatic discharge–charge profiles for Bi–$LiBH_4$–AB composite electrodes in the voltage range of 0.2–1.5 V at 0.1C. Only selected cycles (1, 5, 10, 20, 30, 40, 50, 60, 70, 80, 90, 100) are shown for clear visibility. (b) Cyclic stability of Bi–$LiBH_4$–AB composite electrodes as shown by discharge/charge capacity and the coulombic efficiency *vs.* cycle no.

Bi conversion reaction as shown in eqn (1), resulting in a low polarization and a high initial coulombic efficiency.

$$Bi + Li \leftrightarrow LiBi + 2Li \leftrightarrow Li_3Bi \quad (1)$$

Similarly, Fig. 2(b) shows the first galvanostatic charging–discharging profile of Sb–$LiBH_4$–AB composite electrode using similar electrolyte $LiBH_4$ between 0.2–1.5 V potential window at 0.1C. The first discharge capacity is found to be 657.7 mA h g^{-1} which is very close to the theoretical capacity of Sb (660 mA h g^{-1}), suggesting the non-existence of any side reaction herein. During discharging the first flat plateau corresponding to Sb → Li_2Sb reaction at 0.92 V (up to point 2) is followed by further lithiation plateau at 0.88 V, corresponding to Li_2Sb → Li_3Sb reaction and ends at point 3. These plateaus are also observed in the reverse scan, *i.e.* charging process, and the reverse pattern of the compounds formation occurs. At point 4, Li_3Sb disappears with the appearance of Li_2Sb phase (ESI, Fig. S2†). The next plateau appears immediately after and very close to the first charging plateau, *i.e.* at ∼0.97 V, which suggests the delithiation of Li_2Sb to form Sb with the small unreacted amount of Li_2Sb (point 5). So, according to the above results, the electrochemical reaction mechanism can be represented by the following eqn (2),

$$Sb + 2Li \leftrightarrow Li_2Sb + Li \leftrightarrow Li_3Sb \quad (2)$$

To further explore the capability of the prepared composite electrodes in practical application, the cyclic stability was also investigated under 0.2–1.5 V as shown in Fig. 3 & 4. Fig. 3(a) shows the cyclic galvanostatic discharge–charge profiles of Bi–$LiBH_4$–AB composite electrode for selected no. of cycles up to 100 cycles. The capacity is found to be decreased to 3853.3 mA h cm^{-3} (394 mA h g^{-1}) after 100 cycles from 4681.7 mA h cm^{-3} (478.7 mA h g^{-1}) in the first cycle, as depicted in Fig. 3(b). The stable coulombic efficiency with unchanged plateau potential over no. of cycles also suggests the nice performance of the coin

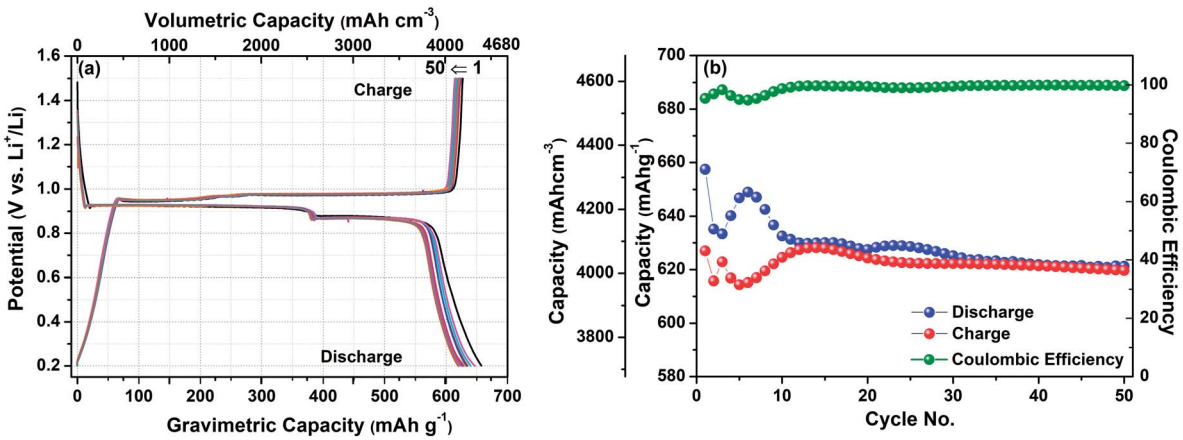

Fig. 4 (a) The cyclic galvanostatic discharge–charge profiles for Sb–$LiBH_4$–AB composite electrodes in the voltage range of 0.2–1.5 V at 0.1C. Only selected cycles (1, 5, 10, 20, 30, 40, 50) are shown for clear visibility. (b) Cyclic stability of Sb–$LiBH_4$–AB composite electrodes as shown by discharge/charge capacity and the coulombic efficiency *vs.* cycle no.

Open Access Article. Published on 29 April 2019. Downloaded on 2/1/2026 9:02:21 AM. This article is licensed under a Creative Commons Attribution-NonCommercial 3.0 Unported Licence.

cell. The capacity became almost stable after 70 cycles. On comparing our results with the available reports, it can clearly be seen that our composite electrode has demonstrated a drastic improvement in the cyclic stability with very high capacity in comparison with the bare Bi nanoparticles with liquid electrolyte [$LiPF_6$ in ethyl methyl carbonate (EMC)/ethylene carbonate (EC)/diethyl carbonate (DEC)] where it exhibits poor cyclic stability and retained only 60 mA h g^{-1} after 100 cycles.[14] Also, the commercially available bulk Bi–C electrode shows a large capacity decay from$\sim$ 650 mA h g^{-1} to around 200 mA h g^{-1} after 100 cycles.[15]

The results are even better with Sb–$LiBH_4$–AB composite electrode, although, the obtained capacity reveals a slight decay in the initial cycles, the coulombic efficiency approaches 95% and is found quite stable only after 20 cycles (Fig. 4). It is interesting to note that the coulombic efficiency was significantly lower in comparison with Bi anode. This could be related to the larger volume change associated with the Sb $\leftrightarrow$ Li_3Sb reaction (135%) in comparison to Bi $\leftrightarrow$ Li_3Bi reaction (42%).[16,17] The large volume change in the lattice generates stress in the lattice, thus making Li-ion diffusion/extraction difficult, which in turn may lower the coulombic efficiency. This large volume expansion took few initial cycles to settle down, which causes the lower coulombic efficiency. After accommodating this volume change in the anode layer the coulombic efficiency became higher and stable. As shown in Fig. 4(b), the initial gravimetric capacity is 4393.4 mA h cm^{-3} (657.7 mA h g^{-1}), which is reduced to 4148.3 mA h cm^{-3} (621 mA h g^{-1}) after 50 cycles with a coulombic efficiency in the range of 90–99%. This is again a significant result as compared to the previous work on bulk as well as nano-based samples, pure Sb–C composite with liquid electrolyte reveals that the capacity faded down to 150 mA h g^{-1} after 50 cycles from the initial capacity of $\sim$750 mA h g^{-1}. However the author resolved this problem by adding Bi in a particular composition as $Bi_{0.57}Sb_{0.43}$-C. $Bi_{0.57}Sb_{0.43}$-C sample delivers an initial delithiation capacity of 410 mA h g^{-1} and cycles stably for 300 cycles with a capacity decay of only 0.09% per cycle.[15] Sb nanoparticles also shows fast capacity decay after 30 cycles. Again, for pure Sb nanoparticles the capacity decay is fast, however Bryngelsson *et al.* demonstrated that their Sb/Sb_2O_3 nanoparticle coatings stabilized at 640 mA h g^{-1} during 50 cycles.[18]

In point of fact, the biggest problem with these anode materials is their volume change during lithiation/delithiation, which generates cracks in the electrode and causes the loss of the connectivity.[19–21] However, in our system, we did not observe any cracks even after cycling (ESI; Fig. S3 and S4†). The elemental mapping suggests that Bi and Sb were present homogeneously throughout the electrode even after cycling. It can be proposed that the presence of $LiBH_4$ along with carbon (AB) works as a binder and provides a cushioning effect thus accommodating the volume change easily, which drastically improved the cyclic stability. In addition to cyclic stability, $LiBH_4$ and AB also enhanced the ionic and electrical conductivity of the anode materials, so that Li-ion can easily diffuse into the anode layer.

Conclusions

In conclusion, we have reported a highly stable performance of Bi & Sb anodes with $LiBH_4$ as a solid electrolyte for all solid-state Li-ion battery. These anode materials exhibit outstanding volumetric capacity and superior stability. The high stability of these systems can be attributed to the cushioning effect of $LiBH_4$ and carbon presented in the composite, which is a feature in addition to their ionic & electrical conductivity respectively. Interestingly, the use of direct bulk material as anode eliminates the need of nanostructures, which are difficult to prepare on a large scale. We have shown the implementation of hydride-based ($LIBH_4$) electrolyte to other anode materials first time, which can open a path to utilize it to other high capacity anode materials and can be helpful for the development of rechargeable LIBs with high-safety.

Conflicts of interest

There are no conflicts to declare.

Acknowledgements

This work was supported by DST, New Delhi (IFA-13/PH-84), SERB, New Delhi (ECR/2016/1780, ECR/2016/1888) and UGC-DAE CSR (CSR-IC-MSRSR-23/CRS-231/2017-18/1312, CSR-IC/CRS-73/2014-15/581).

References

1 P. E. de Jongh, D. Blanchard, M. Matsuo, T. J. Udovic and S. Orimo, *Appl. Phys. A: Mater. Sci. Process.*, 2016, **122**, 251.
2 J. C. Bachman, S. Muy, A. Grimaud, H.-H. Chang, N. Pour, S. F. Lux, O. Paschos, F. Maglia, S. Lupart, P. Lamp, L. Giordano and Y. Shao-Horn, *Chem. Rev.*, 2016, **116**, 140–162.
3 L. Zeng, T. Ichikawa, K. Kawahito, H. Miyaoka and Y. Kojima, *ACS Appl. Mater. Interfaces*, 2017, **9**, 2261–2266.
4 K. Kawahito, L. Zeng, T. Ichikawa, H. Miyaoka and Y. Kojima, *Mater. Trans.*, 2016, **57**, 755–757.
5 L. Zeng, K. Kawahito, S. Ikeda, T. Ichikawa, H. Miyaoka and Y. Kojima, *Chem. Commun.*, 2015, **51**, 9773–9776.
6 M. Yoshio, H. Wang and K. Fukuda, *Angew. Chem.*, 2003, **115**, 4335–4338.
7 Y. Guo, Y. Wei, H. Li and T. Zhai, *Small*, 2017, **13**, 1701649.
8 J. He, Y. Wei, T. Zhai and H. Li, *Mater. Chem. Front.*, 2018, **2**, 437–455.
9 N. Nitta and G. Yushin, *Part. Part. Syst. Charact.*, 2014, **31**, 317–336.
10 J. Ni, X. Bi, Y. Jiang, L. Li and J. Lu, *Nano Energy*, 2017, **34**, 356–366.
11 N. Nitta, F. Wu, J. T. Lee and G. Yushin, *Mater. Today*, 2015, **18**, 252–264.
12 C.-M. Park, S. Yoon, S.-I. Lee and H.-J. Sohn, *J. Power Sources*, 2009, **186**, 206–210.
13 F. Yang, F. Yu, Z. Zhang, K. Zhang, Y. Lai and J. Li, *Chem.–Eur. J.*, 2016, **22**, 2333–2338.

 This journal is © The Royal Society of Chemistry 2019

Open Access Article. Published on 29 April 2019. Downloaded on 2/1/2026 9:02:21 AM.
This article is licensed under a Creative Commons Attribution-NonCommercial 3.0 Unported Licence.

14 Y. Zhong, B. Li, S. Li, S. Xu, Z. Pan, Q. Huang, L. Xing, C. Wang and W. Li, *Nano-Micro Lett.*, 2018, **10**, 56.
15 Y. Zhao and A. Manthiram, *Chem. Mater.*, 2015, **27**, 3096–3101.
16 C.-F. Sun, J. Hu, P. Wang, X.-Y. Cheng, S. B. Lee and Y. Wang, *Nano Lett.*, 2016, **16**, 5875–5882.
17 A. Darwiche, C. Marino, M. T. Sougrati, B. Fraisse, L. Stievano and L. Monconduit, *J. Am. Chem. Soc.*, 2012, **134**, 20805–20811.
18 H. Bryngelsson, J. Eskhult, L. Nyholm, M. Herranen, O. Alm and K. Edstrom, *Chem. Mater.*, 2007, **19**, 1170–1180.
19 X. Zhang, F. Lai, Z. Chen, X. He, Q. Li and H. Wang, *Electrochim. Acta*, 2018, **283**, 1689–1694.
20 Y. Yu, J. Liu, L. Yu, C. Wu, Y. Wen, K. Yin, F.-K. Chiang, R. Hu, J. Liu, L. Sun, L. Gu, J. Maier and M. Zhu, *Nano Lett.*, 2017, **3**, 2034–2042.
21 R. Dai, Y. Wang, P. Da, H. Wu, M. Xu and G. Zheng, *Nanoscale*, 2014, **6**, 13236–13241.